Fibril Structure Demonstrates the Role of Iodine Labelling on a Pentapeptide Self-Assembly

Alessandro Marchetti+,[a] Andrea Pizzi+,[a] Greta Bergamaschi,[b] Nicola Demitri,[c] Ulrike Stollberg,[d] Ulf Diederichsen,[d] Claudia Pigliacelli,*[a] and Pierangelo Metrangolo*[a]

Abstract: Iodination has long been employed as a successful labelling strategy to gain structural insights into proteins and other biomolecules *via* several techniques, including Small Angle X-ray Scattering, Inductively Coupled Plasma Mass Spectrometer (ICP-MS), and single-crystal crystallography. However, when dealing with smaller biomolecular systems, interactions driven by iodine may significantly alter their self-assembly behaviour. The engineering of amyloidogenic peptides for the development of ordered nanomaterials has greatly benefitted from this possibility. Still, to date, iodina-tion has exclusively been applied to aromatic residues. In this work, an aliphatic bis-iodinated amino acid was synthesized and included into a custom pentapeptide, which showed enhanced fibrillogenic behaviour. Peptide single crystal X-ray structure and powder X-ray diffraction on its dried water solution demonstrated the key role of iodine atoms in promoting intermolecular interactions that drive the peptide self-assembly into amyloid fibrils. These findings enlarge the library of halogenated moieties available for directing and engineering the self-assembly of amyloidogenic peptides.

Introduction

Single and multiple isomorphous replacement with metals or halogens has historically been the most common approach for phasing of complex biomolecules such as proteins.[1–3] Despite the development of more accurate and less invasive techniques based on anomalous dispersion,[4–6] heavy-atom labelling is still employed for niche applications, including RNA tagging and defects visualization on zeolites surfaces, labelling for Small Angle X-Ray Scattering (SAXS) and Inductively Coupled Plasma

[a] A. Marchetti,+ Dr. A. Pizzi,+ Dr. C. Pigliacelli, Prof. P. Metrangolo
     Laboratory of Supramolecular and Bio-Nanomaterials (SBNLab)
     Department of Chemistry, Materials, and Chemical Engineering "Giulio Natta"
     Politecnico di Milano
     Via L. Mancinelli 7, 20131 Milano (Italy)
     E-mail: claudia.pigliacelli@polimi.it
             pierangelo.metrangolo@polimi.it

[b] Dr. G. Bergamaschi
     Istituto di Scienze e Tecnologie Chimiche
     National Research Council of Italy
     Via M. Bianco 9, 20131 Milano (Italy)

[c] Dr. N. Demitri
     Elettra – Sincrotrone Trieste
     S.S. 14 Km 163.5 in Area Science Park, 34149 Basovizza – Trieste (Italy)

[d] Dr. U. Stollberg, Prof. U. Diederichsen
     Institute for Organic and Biomolecular Chemistry
     Georg-August-University Göttingen
     Tammannstr. 2, 37077 Göttingen (Germany)

[+] These authors contributed equally to this work.

📱 Supporting information for this article is available on the WWW under https://doi.org/10.1002/chem.202104089

Mass Spectrometer (ICP-MS).[7–11] More recently, we extended the use of iodine as heavy-atom label for transmembrane β-peptides, to infer conformational parameters of lipid membranes by means of X-ray diffraction.[12,13] Using iodine-labelled amino acids as markers, it was possible to precisely identify an iodinated residue in the lipid membrane and, consequently, probe structural changes occurring in the helical transmembrane domain.[13]

Beside this methodological applications, iodination has recently received growing interest in nanomaterials science[14–17] and supramolecular chemistry[18–20] as minimal, yet impactful, single-point mutation for small molecules such as peptides.[21,22] This interest arose from the ability of a covalently bonded iodine atom to engage in diverse noncovalent interactions as both Lewis base and Lewis acid. Indeed, its polarizability results in an intrinsic amphoteric behaviour, which allows it to simultaneously engage in both hydrogen (HB) and halogen bonds (XB), according to the surrounding chemical environment.[23,24]

Owing to its distinctive features, iodine has been proven to impact self-assembly[25,26] and crystallization[27,28] of amyloidogenic peptides, short amino acid sequences that retain the peptide full capability of assembling into amyloid fibrils (e.g., the NFGAIL sequence of the human islet amyloid polypeptide (hIAPP)[29] and the DFNKF sequence of the human calcitonin (hCT) hormone[30]). Specifically, some of us recently demonstrated that both crystallogenic and fibrillogenic behaviour are enhanced with respect to the non-iodinated counterparts, when iodination is performed on the *para*-position of peptides' aromatic residues.[25,31] Indeed, XB contribution alters the inter- and intramolecular interactions between side chains, exacerbating peptides' self-assembly propensity and promoting their hydrogelation properties.[25,31] Further, iodine presence in aromatic residues can assist the stabilization of the overall

Chemistry–A European Journal

Research Article
doi.org/10.1002/chem.202104089

Chemistry Europe
European Chemical
Societies Publishing

molecular packing, favouring the orientation of the aromatic rings towards the formation of π-π interactions or by stabilizing T-shape arrangements through HB.[32,33] Still, the impact of iodination of aliphatic residues in amyloidogenic peptides has not been studied, to date, and the possible role of XB in the resulting peptide self-assembly pattern remains, therefore, unexplored.[34,35]

Moreover, in peptide science, whether crystal structures can be related to the peptide packing in the fibril phase is still under debate.[36,37] According to the nature of the chosen solvents and solute, both the fibrillar and the crystal states can be thermodynamically stable for amyloidogenic peptides.[38] In this sense, we reasoned that the additional noncovalent interactions mediated by iodine atoms could represent a tool to tune the competition between crystallization and fibrils formation.

Thus, in this work, we introduced a custom bis-iodinated aliphatic amino acid into a tailor-made peptide, derived from the amyloidogenic sequence DFNKF,[30,39] and probed the ability of the newly obtained peptide to self-assemble into amyloid fibrils and form crystalline structures. Notably, the iodinated residue also endowed the peptide with a new functionality, rendering it a good Au-reducing agent. Iodine impact on fibrillar self-assembly, crystallogenic ability, and Au-reducing properties was assessed employing the non-iodinated counterpart as a reference molecule. Importantly, peptide single crystals obtained from water and the dried fibrils showed the same core fibril features, thus demonstrating the key role of iodine atoms in promoting intermolecular interactions that drive the peptide self-assembly into amyloid fibrils.

Results and Discussion

Amino acid design and single crystal X-ray structure

Self-assembly of amyloidogenic peptides is typically dictated by noncovalent interactions such as HBs, hydrophobic forces, and π-π stacking. Aromatic amino acids are commonly found in core motifs of fibril-forming peptides where they significantly contribute to both formation kinetics and thermodynamic stability of the assembled structures.[40–42] Despite amyloidogenic sequences being entirely made of aliphatic amino acids are less commonly found, aliphatic residues and sequences can also contribute to the typical amyloid self-assembly.[34] In fact, a combination of aliphatic and aromatic side chains usually leads to the strongest networks of noncovalent interactions.[35]

To uncover the impact of iodination on aliphatic amino acids' self-assembly properties, we decided to exploit for our investigation a previously synthesized[13] diiodo-allylglycine ($AllG(I_2)$) (Figure 1a). Iodine was the halogen of choice as XB strength increases with halogen atom polarizability, thus rendering iodine-mediated XBs stronger than interactions given by other halogens. A commercially available allylglycine (AllG) was used as reference amino acid, to better assess iodine atoms' role in $AllG(I_2)$ intermolecular interactions and self-assembly behaviour.

Our studies began with investigating the $AllG(I_2)$ single crystal X-ray structure. In detail, the iodinated amino acid crystallized from a water/isopropanol mixture in the $P2_1$ space group, where two $AllG(I_2)$ and one isopropanol molecule compose the asymmetric unit (ASU, Figure S3). Amino acid molecules interact with each other by means of strong and reciprocal HBs that involve their charged termini (Figure 1b), forming very compact dimers. Of note, the same dimers are further stabilized by type II halogen bonds, thus confirming the amphoteric behaviour of iodine atoms in this amino acid moiety. Indeed, one of the iodine atoms of an $AllG(I_2)$ unit displays electrophilic behaviour on the extension of the C—I bond, interacting with the electron rich belt of another iodine atom belonging to a facing $AllG(I_2)$ molecule. In detail, I2 behaves as a XB-donor and I3 acts as an acceptor, with a distance of 3.695(3) Å. The normalized contact (Nc), corresponding to the ratio between the contact distance and the sum of the VdW radii of the two atoms involved in the contact, is 0.93. The value of the C1—I2···I3 angle (167.7(8)°) qualifies the nature of this contact as a XB. Further evidence of the amphoteric attitude of iodine atoms, as a consequence of the anisotropic
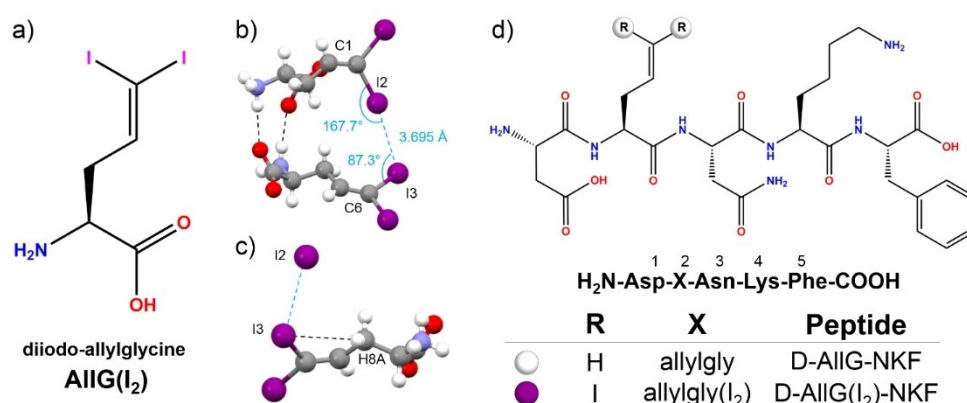

Figure 1. a) Chemical structure of diiodo-allylglycine ($AllG(I_2)$); Single crystal X-ray structure of $AllG(I_2)$ highlighting iodine-mediated b) intermolecular XBs (sky-blue dashed lines) and HBs and c) intramolecular HBs (black dashed lines); d) $D-AllG(I_2)$-NKF and D-AllG-NKF chemical structures. Colour code: C, grey; O, red; N, blue; I, purple; and H, white.

Chemistry–A European Journal

Research Article
doi.org/10.1002/chem.202104089

Chemistry Europe
European Chemical
Societies Publishing

distribution of the electron density around their surfaces, is the angle C6–I3⋯I2 (87(1)°), almost close to orthogonality, which is in line with a typical type II I⋯I contact, i.e., a XB. In addition, the electron rich belts of I2 and I3 give rise to intramolecular HBs with the methylene groups (Figure 1c), fixing the conformation of the **AllG(I₂)** backbone, hence helping crystallization.

Also, iodine atom I1 displays a short contact with the oxygen atom of a solvent molecule (Figure S4). Although the quality of the diffraction data makes the description of this specific interaction nontrivial, the observed geometrical arrangement suggests that iodine atoms of this moiety can act as XB-donors towards oxygen atoms; this is a key aspect to be considered once this amino acid is inserted in the context of a peptide sequence, where many oxygens are present.

Notably, as previously reported, single crystal X-ray structure of the non-iodinated **AllG(I₂)** analogue, i.e., **AllG** (Refcode: XADTUR[43]), is characterized by non-reciprocal HBs between their charged termini. This leads to the absence of tightly bound dimers, further confirming the key role of iodine atoms in promoting ordered packing in **AllG(I₂)** molecules.

Peptide self-assembly

Given the observed **AllG(I₂)** crystallization ability, we reasoned that by including this amino acid in a natural amyloidogenic sequence (details about synthetic procedures are provided in the Supporting Information), the occurrence of XBs and HBs between peptide strands could be achieved. DFNKF, core motif of the human calcitonin hormone, was chosen as model sequence, as its fibril-forming propensity has extensively been characterized.[25,30] To assess the actual impact of **AllG(I₂)** insertion, we firstly studied **D-AllG(I₂)-NKF** fibrillogenic and crystallogenic behaviour and employed as controls the non-iodinated allylglycine, **AllG**, and the corresponding pentapeptide derived from DFNKF, i.e., **D-AllG-NKF**. Importantly, all the studied peptides carried free amino (N) and carboxyl (C) termini.

Both custom pentapeptides **D-AllG(I₂)-NKF** and **D-AllG-NKF** (Figure 1d) were obtained through a classic solid-phase peptide synthesis approach and their self-assembly behaviour was thoroughly characterized upon dissolution in Milli-Q water.

First, Congo Red (CR) staining studies were carried out and, as shown in Figure 2b, strong and diffused green-gold birefringence could be observed under polarized light solely for **D-AllG(I₂)-NKF**. Specifically, the iodinated peptide presented a dense network of amyloid fibrils clearly visible by optical microscope, in accordance with the formation of long-range cross-β structure.[44] On the other hand, **D-AllG-NKF** sample showed green/blue birefringence[45] solely on the outer boundary of the analysed droplets, suggesting only limited occurrence of β-sheet structures mainly caused by drying-induced aggregation (Figure S6 from e to h).

Following CR studies, peptides' ability to form amyloidal fibrils in solution was further tested and attempts to study their
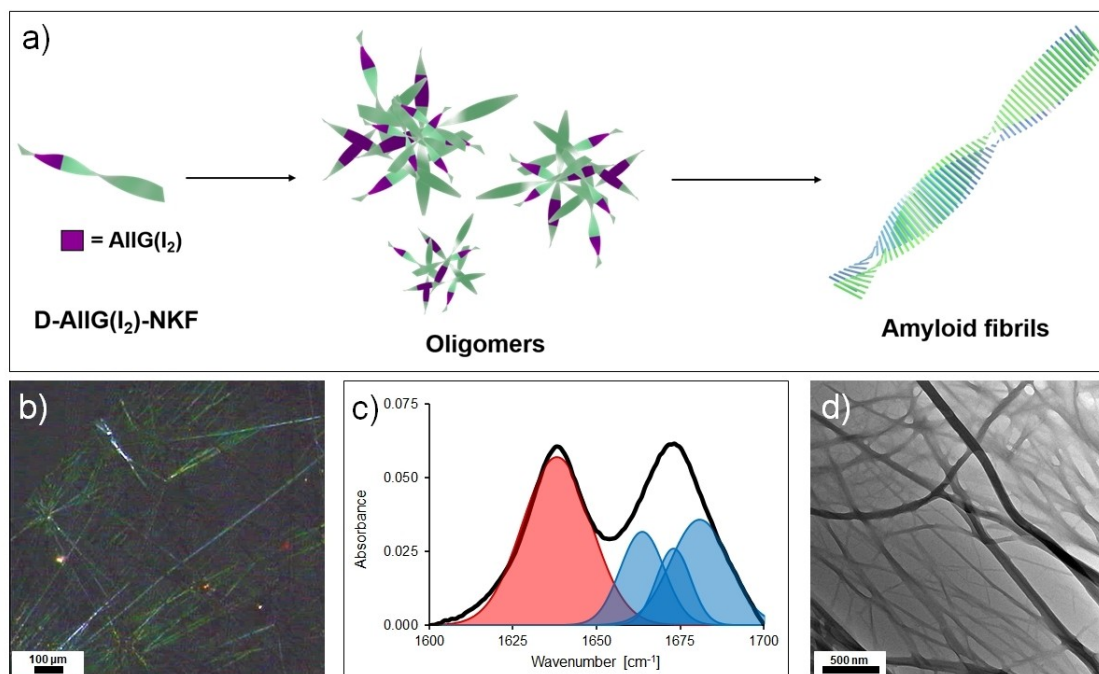

Figure 2. a) Cartoon representing the three main stages of the D-AllG(I₂)-NKF self-assembly process: first, individual peptide molecules (left) combine each other in solution forming spiky intermediate aggregates (center), which then act as nucleation centres for protofibrils to branch out and develop into amyloid fibrils (right); b) Optical microscopy image of a 0.75 mM D-AllG(I₂)-NKF solution stained with Congo Red under polarized light; c) Enlarged amide I region (1600–1700 cm⁻¹) of the ATR-FTIR spectrum (black curve) with Gaussian fitting (coloured curves) of a 0.75 mM D-AllG(I₂)-NKF solution incubated 1 h at 60 °C and aged for 24 h at room temperature. The red curve is associated with a β-sheet secondary structure, whereas the blue curves are related to random coils or β-turns; d) TEM image of a 0.75 mM D-AllG(I₂)-NKF solution incubated 1 h at 60 °C and aged for 24 h.

Chemistry–A European Journal

Research Article
doi.org/10.1002/chem.202104089

Chemistry Europe
European Chemical
Societies Publishing

assembly kinetics through Thioflavin T (ThT) staining were performed. Over the course of analysed timeframe, no increase in fluorescence was observed upon mixing the peptides' solutions with ThT. This result is not entirely surprising, since the inability of DFNKF to bind this marker dye is well-established in literature, even under known fibrillating conditions.[25,46] Thus, a similar behaviour can be expected for analogous sequences composed by the same number of amino acids. The different outcomes of the two staining experiments can be explained considering CR and ThT binding modes. Despite being still debated, it has been shown that ThT emits its characteristic fluorescent signal only when bound as a planar monomer to a properly sized cavity. CR, instead, only requires to be aligned parallelly with respect to the fibrils axis to display its green birefringence under polarized light.[47]

Fibrils morphological evolution in solution over time was also probed *via* circular dichroism (CD). Both **D-AllG(I₂)-NKF** and **D-AllG-NKF** spectra were characterized by a positive peak at 196 nm, a negative peak at 205 nm, and another positive peak at 218 nm. In addition, **D-AllG(I₂)-NKF** spectra presented a broad peak around 238 nm, which was not observed in **D-AllG-NKF** CD profile (Figure S7). No significant shifts were seen over time for the two peptides, in any of the concentration conditions analysed. This could be due to the well-known perturbation caused by aromatic groups in the far UV region, which frequently renders secondary structures evaluations by CD spectra not straightforward.[48]

To gather more insights about **D-AllG(I₂)-NKF** and **D-AllG-NKF** supramolecular behaviours, the formation of secondary structures was probed by attenuated total reflectance-Fourier transformed infrared (ATR-FTIR) spectroscopy and, for both peptides, spectra were acquired from (1) bulk powders and (2) solid films resulting from the evaporation of aqueous solutions dropped directly on the ATR crystal. The amide I region shows a peak at $1640\ cm^{-1}$ and $1630\ cm^{-1}$ for **D-AllG(I₂)-NKF** and **D-AllG-NKF** bulk powders, respectively (Figure S8), possibly indicating the presence of β-sheet secondary structures resulting from local preaggregation phenomena occurring in the solid state. However, solutions analysed after 24 and 72 h of incubation, revealed a different behaviour for the two peptides. Indeed **D-AllG(I₂)-NKF** solution showed a consistent redshift of the $1640\ cm^{-1}$ band with respect to the bulk powder, under every condition analysed, behaviour that was not observed for the **D-AllG-NKF** samples. Upon secondary structure formation, carbonyl oxygens involved in peptide bonding can interact with available electropositive sites, like HB- and XB-donors, leading to intermolecular vibrational coupling. This results in electronic depletion of the carbonyl group, which justifies the observed redshifts.[21,49] Additionally, Gaussian fitting of **D-AllG(I₂)-NKF** spectrum (Figure 2c and Table S3) corroborated the attribution of the $1635\ cm^{-1}$ band to a β-sheet secondary structure and confirmed the presence of β-turns and bound trifluoroacetate counterions, as indicated by the peak at around $1660\ cm^{-1}$ and $1673\ cm^{-1}$, respectively[50].

Following spectroscopic studies, the morphologies of peptides' self-assembled structures formed in Milli-Q water solutions were probed *via* transmission electron microscopy (TEM).

As shown in Figure S10, images acquired on **D-AllG-NKF** samples do not show any structured aggregate, confirming its inability to form ordered nanostructures in any of the studied experimental conditions. Being devoid of iodine atoms on the aliphatic residue, **D-AllG-NKF** is unable to form iodine-mediated XBs or HBs, and to develop an organized supramolecular structure. Conversely, **D-AllG(I₂)-NKF** samples clearly showed a morphological evolution over time which was strongly impacted by sample concentration, incubation time, and temperature. Specifically, the most concentrated samples (0.75, 1, and 2 mM) developed structured and widely interdigitated fibrillar networks (Figure 2d and Figure S11), with 0.75 mM being identified as the minimum concentration threshold for fibrils formation. The observed self-assembly pattern unfolds across three core stages (Figure 2a), with the transition from individual peptide molecules to fully developed amyloid fibrils being mediated by the formation of aggregates characterized by a spiky interface (Figure S11). These irregular oligomers act as nucleation centres for undeveloped protofibrils to branch out.[51]

Assuming the kinetics of fibrils growth to be described by an Arrhenius-like equation,[52] higher incubation temperature was expected to significantly impact fibrils formation and growth, leading to larger extent of structuring and to a denser network formation. Indeed, short incubation at higher temperature was enough to accelerate **D-AllG(I₂)-NKF** assembly, leading to the formation of extensive fibrillar networks already after 24 h. Differently, whenever heating was not performed, fully developed fibrils could be observed in all samples only after 72 h from dissolution.

Iodinated peptide single crystal X-ray structure

Iodine involvement in promoting amyloid fibrils formation was further studied by X-ray diffraction analysis. Crystals of **D-AllG(I₂)-NKF** were successfully obtained from water solutions by slow solvent evaporation at room temperature, over a period of 6 months. Grown crystals were small and weakly diffracting, as it was previously reported for other halogenated crystals,[31,33] thus accurate structure solution was achievable only using synchrotron radiation.

D-AllG(I₂)-NKF crystallizes in the chiral monoclinic $P2_1$ space group with two peptide molecules in the ASU (Figure S13). Similarly to other amyloidogenic peptides, its crystal structure shows the typical cross-β-spine formed by a pair of β-sheets,[53] each of which is constituted by elongated strands stacking parallelly with respect to the spine axis. β-sheets share a common dry interface stabilized by the interdigitation of complementary side chains, called "steric zipper".[54,55] β-sheets forming the zipper stack along the crystallographic *b* axis at a distance of 12.44(5) Å, which is typical for amyloid systems. The zipper (Figure 3a) belongs to the "class 2", which is defined as a "face-to-back, up-up" zipper. This motif consists in a parallel arrangement within a single β-sheet, C-to-C symmetry (i.e., parallel arrangement between facing beta sheets) and face-to-back pairing among the sheets forming the zipper.[54]
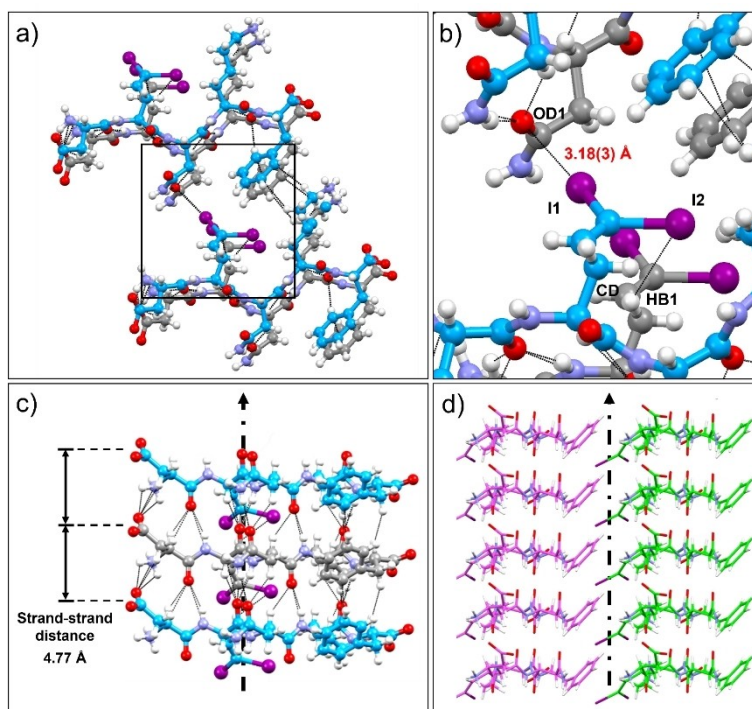
Chemistry–A European Journal

Research Article
doi.org/10.1002/chem.202104089

**Chemistry
Europe**
European Chemical
Societies Publishing

Figure 3. a) Steric zipper class 2 motif formed by D-AllG(I₂)-NKF; b) Zoomed view of the steric zipper where an intermolecular halogen bond occurs between one iodine atom (I1) of the AllG(I₂) residue and the carbonyl group of an asparagine residue belonging to an adjacent β-sheet (OD1), and the hydrogen bond between the other iodine atom of the AllG(I₂) residue (I2) and a hydrogen belonging to a different strand of the same β-sheet (HB1); c) Lateral view of an individual β-sheet highlighting the 4.77 Å distance between centroids of stacked strands. The axis reported corresponds to the crystallographic *a* axis; d) Lateral view of parallel β-sheet, developing along the crystallographic *a* axis. Colour code: C, grey and cyan in a), b) and c), magenta and green in d); O, red; N, blue; I, purple; and H, white.

Each strand is composed by **D-AllG(I₂)-NKF** monomers in their fully extended conformation, each engaging in a network of N–H···O HBs with neighbouring strands belonging to the same β-sheet architecture (Figure 3c). The resulting peptide stacking, growing parallel to the crystallographic *a* axis (Figure 3d), gives origin to a strand-strand distance of 4.77(1) Å, which is in accordance with the typical packing parameters of amyloid fibrils and with the values found from powder X-ray analysis.[33,54] Lateral packing (Figure S15) is driven by salt bridges involving the C-terminus and the lysine side-chain, and between the protonated N-terminus and the aspartate side chains of flanked molecules (average $-COO^-···NH_3^+$ distance approximately equal to 3 Å). This set of electrostatic interactions drives the pairing of flanked β-pleated sheets along the crystallographic *c* axis.

D-AllG(I₂)-NKF crystal structure confirms the amphoteric behaviour of iodine atoms, in agreement with the X-ray data of the single **AllG(I₂)** amino acid. Indeed, in the dense network of intra- and intermolecular HBs, iodine atoms contribute to both the stabilization of the steric zipper and the β-sheets packing by engaging in HBs and XBs with different strands. Namely, iodine atoms confer both *intra*- and *inter*-sheet stabilization to this amyloid structure. In detail, the two iodine atoms of the **AllG(I₂)** residue show different patterns of interaction, with one iodine (I1, Figure 3b) being involved in an intermolecular XB with the amide oxygen (OD1) of the asparagine side chain of a facing strand. The second one (I2, Figure 3b), instead, engages in a HB with the sp^2 moiety of an underneath strand. I1···OD1 distance is 3.18(3) Å, while C–I1···OD1 and C–I2···HB1 angles have values of 166(1)° and 70(1)°, respectively. The directionality of XB and HB involving the two iodine atoms highlights the electron density anisotropy associated to iodine atoms. Indeed, XB occurs along the extension of the C–I bond where a region of positive potential (σ-hole) is located, whereas the negative potential around the equatorial region enables the HB. The I1···OD1 distance, well below of the sum of the VdW radii of I and O, i.e., 3.50 Å, and the good linearity of the contact angle confirm that the I1···OD1 interaction occurs *via* XB. These findings clearly establish the role of the aliphatic iodinated residue in promoting **D-AllG(I₂)-NKF** self-assembly into amyloid fibrils. I2 iodine atom, despite not engaging in any XB, favours the stabilization of the β-sheet through *inter*-strand HBs. Moreover, as in the crystal structure of the **AllG(I₂)** amino acid, the iodine atoms in the **D-AllG(I₂)-NKF** peptide form the same intramolecular HBs with the -CH₂ moieties. The normalized contact (Nc) of I1···OD1 synthon is equal to 0.91. Previously reported Nc value for aromatic residues of the amyloidogenic sequence KLVF(I)F(I), which shows a similar I···O interaction with respect to the one identified in the **D-AllG(I₂)-NKF**, is equal to 0.96.[31] The observed lower Nc demonstrates that the I···O contact formed by **D-AllG(I₂)-NKF** is stronger, providing a

Chemistry–A European Journal

Research Article
doi.org/10.1002/chem.202104089

Chemistry Europe
European Chemical
Societies Publishing

further evidence of the ability of the iodinated aliphatic residue to stabilize amyloid fibrils.

Interesting insights arise from the comparison between the crystal structures of **D-AllG(I₂)-NKF** and its di-halogenated analogues DF(Cl)NKF(Cl) and DF(I)NKF(I), recently reported.[32] Despite the different residues in positions 2 and 5, crystal structures superimposition (Figure S16) shows that the three peptides share similar structural and geometrical features, achieving a root mean square deviation (RMSD) between the overlapped amino acids of 1.31 Å. As a confirmation of this similarity, all three peptides show a "class 2" steric zipper.[32]

Notably, despite the similarities, the role played by halogen atoms in DF(I)NKF(I) and DF(Cl)NKF(Cl) structures is different with respect to the one observed **D-AllG(I₂)-NKF**. In fact, DF(I)NKF(I) iodine atoms engage in XBs exclusively with water molecules, stabilizing the β-sheet only through HBs between adjacent strands. Cl atoms in DF(Cl)NKF(Cl), instead, are not engaged in any relevant noncovalent interaction.[32] Differently, **D-AllG(I₂)-NKF** presents aliphatic iodinated side chains whose iodine atoms behave as amphoteric species, by prompting both HBs and XBs between peptide molecules, which are of primary relevance in driving the peptide assembly. Thus, among the three derivatives of the DFNKF sequence, **D-AllG(I₂)-NKF** represents the only example in which the iodine atoms are involved in XBs that actively stabilize the cross-β spine architecture.

Dried fibrillar solution characterization

Given such a distinctive crystallogenic ability, we reasoned that **D-AllG(I₂)-NKF** spontaneous self-assembly into amyloidal fibrils could also be associated with the stabilization of a partially crystalline structure, possibly consistent with the peptide polymorph observed by single crystal X-ray studies. We therefore investigated the possible crystallinity of self-assembled **D-AllG(I₂)-NKF** fibrils *via* scanning electron microscopy (SEM) and powder X-ray diffraction (PXRD). In detail, a 0.75 mM **D-AllG(I₂)-NKF** solution was incubated for 72 h and lyophilized, and the obtained dry powder was analysed to correlate sample's features at the micrometric scale with its organization at the angstrom scale. Comparison between SEM images of **D-AllG(I₂)-NKF** samples acquired prior and after fibrillation and lyophilization, clearly emphasises radical changes in its packing. Indeed, SEM images of pristine peptide (Figure 4a and Figure S12), as obtained right after synthesis, reveal an amorphous morphology, with jagged and irregular surfaces, indicating the absence of a long-range supramolecular ordering (Figure S10). More crystalline structures could, instead, be observed in SEM images acquired for the fibrillated and lyophilized **D-AllG(I₂)-NKF** sample (Figure 4b), confirming that the combination of incubation in aqueous solution and subsequent lyophilization strongly increases the degree of structural ordering, as expected when fibrillation takes place.[56,57] The transition towards a crystalline packing is further stressed by the comparison between PXRD pattern (Figure 4c) of the bulk powder, which displays only a shallow and broad peak, and of the fibrillated and lyophilized peptide, characterized by sharp and well-defined peaks. By comparison, applying the same treatment to the non-iodinated **D-AllG-NKF** did not lead to any crystallinity increase (Figure S17), thus underlining the relevance of iodine and iodine-mediated interactions in the self-assembly process.

Importantly, superimposition between PXRD pattern obtained from the fibrillated and lyophilized **D-AllG(I₂)-NKF** sample and the one simulated from its single crystal X-ray structure indicates that, in both cases, the core structural features of fibrils are preserved, as testified by the elevated similarity between the two powder patterns at 2θ values lower
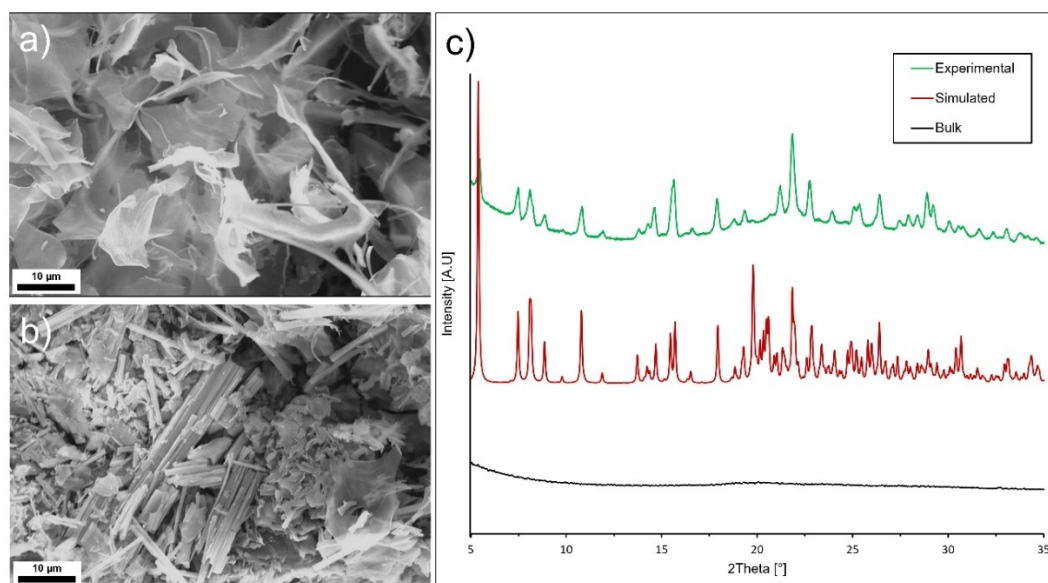

Figure 4. SEM images of a) bulk and b) fibrillated and lyophilized D-AllG(I₂)-NKF; c) Powder X-ray diffraction spectra of D-AllG(I₂)-NKF as a bulk powder (black), after fibrillation and lyophilization (green), and simulated from the single crystal X-ray structure (red).

Chemistry–A European Journal

Research Article
doi.org/10.1002/chem.202104089

Chemistry
Europe
European Chemical
Societies Publishing

than 20°. Relevant examples are the peak at $2\theta = 18.7°$, corresponding to the (1,0,1) Miller plane and representative of the HB-based peptide stacking, and the peak at $2\theta = 5.5°$ related to the (0,0,4) Miller plane and consistent with the interface between two flanked peptide units growing along *c* axis. This finding justifies the extrapolation of the single crystal X-ray structure to the fibril state.[37]

Iodine-mediated Au reduction

Owing to their ability to behave as capping and reducing agents, peptides have often been used as efficient templates for controlling the synthesis and self-assembly of gold nanoparticles, promoting a controlled nucleation and growth of gold nanostructures[58–60] or tuning their properties.[61] When dealing with amyloidogenic peptides, though, the interaction occurring between gold atoms and peptide monomers can compete with peptides' self-assembly pathway towards fibrils, often leading to the development of different structural arrangements.[62–64]

Iodinated compounds have been reported for their ability to reduce gold salts.[65] Moreover, iodination of amyloidogenic peptides was recently developed as a strategy to obtain gold-peptide superstructures.[15] The key step of such reactivity was the activation of the —C—I bond on an iodobenzene moiety promoted by Au(I).[66–68]

Although, to date, gold reducing ability has been reported only for iodinated peptide bearing iodine atom(s) on aromatic residues, the iodinated side chain of **D-AllG(I₂)-NKF** could in principle be exploited to mediate gold reduction. To investigate this possibility, an equimolar aqueous solution of **D-AllG(I₂)-NKF** and HAuCl₄ was incubated for 1 h at 60°C, in accordance to previously developed one-pot procedure.[15] **D-AllG-NKF** solutions were incubated under the same conditions, as control samples. As expected, after incubation, **D-AllG(I₂)-NKF@Au** sample was characterized by a red/pink colour, whereas **D-AllG-NKF@Au** sample remained perfectly colourless, meaning that the absence of the iodinated moiety renders the latter peptide unreactive towards Au(III). TEM analysis of **D-AllG(I₂)-NKF@Au** samples (Figure 5b and Figure S18) confirmed the formation of gold nanostructures (i.e., spheres, rods, triangle, pentagons, hexagons) in solutions, mostly embedded in a peptide matrix. As expected, Au-peptide interactions during incubation hindered the characteristic fibrillar self-assembly, thus preventing the formation of mature peptide fibrils. Despite the lack of an overall supramolecular organization between the Au and the peptide, **D-AllG(I₂)-NKF@Au** UV-vis spectrum (Figure 5c) clearly shows the presence of a surface plasmon resonance peak at 532 nm, confirming the occurrence of gold reduction to its metallic state and the formation of gold nanostructures. Although more studies are needed to better control the reduction process and tune the gold nanostructures morphologies, these preliminary results demonstrate the ability of iodinated aliphatic residues in promoting peptide-mediated gold reduction, thus enlarging the library of peptide-based templates for gold nanomaterials design.
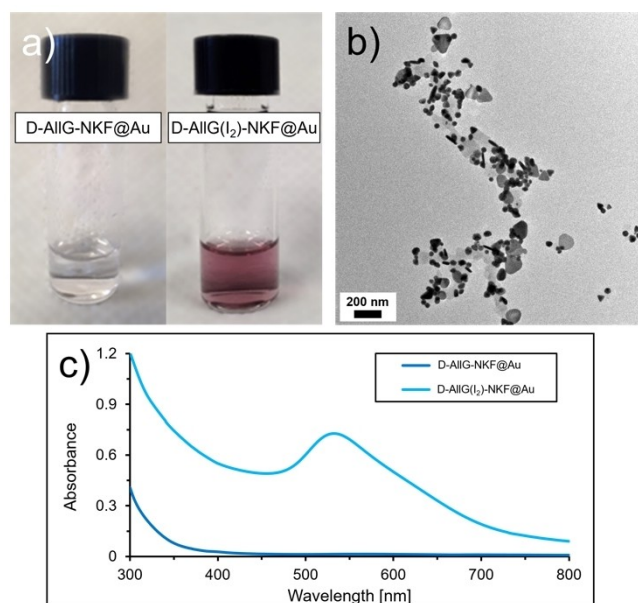

Figure 5. a) D-AllG-NKF@Au and D-AllG(I₂)-NKF@Au samples images; b) TEM image of D-AllG(I₂)-NKF@Au; c) UV-vis spectra of D-AllG-NKF@Au and D-AllG(I₂)-NKF@Au samples.

Conclusions

Iodine has historically been one of the reference atoms for protein labelling, owing to its high electron density and to iodination having minimal impact on molecules primitive cell. However, given its ability to form HB and XB interactions, iodine represents a powerful tool in supramolecular chemistry for driving self-assembly of diverse building blocks. In the last years, this reasoning has successfully been applied to engineer amyloidogenic peptides able to form structured nanomaterials. Nevertheless, the impact of iodination on aliphatic residues has, to date, remained unexplored in such a context.

In this study, we investigated the impact of iodination on the aliphatic residue of a tailor-made pentapeptide, **D-AllG(I₂)-NKF**, derived from the amyloidogenic sequence DFNKF. We demonstrated that iodination is a minimal yet relevant modification of a pentapeptide, when performed on an aliphatic residue, enhancing the fibrillogenic behaviour at very low concentrations and promoting crystalline packing. **D-AllG(I₂)-NKF** ability to self-assemble into interdigitated amyloid fibrils at low concentrations was confirmed by TEM, Congo Red staining, and ATR-FTIR. High-resolution X-ray crystal structure of **D-AllG(I₂)-NKF** demonstrated the crucial role of iodine atoms in stabilizing the steric zipper. Notably, the non-halogenated counterpart, **D-AllG-NKF**, did not display any sign of fibrillar aggregates formation or crystallinity, highlighting the key role played by iodine in **D-AllG(I₂)-NKF** supramolecular behaviour, as demonstrated by peptide single crystal X-ray structures and powder X-ray diffraction on the dried fibrils, which share the same fibril structure. Additionally, iodination endowed **D-AllG(I₂)-NKF** with Au-reducing properties that leads to the formation of gold nanostructures through a one-pot procedure.

Chemistry–A European Journal

Research Article
doi.org/10.1002/chem.202104089

**Chemistry
Europe**
European Chemical
Societies Publishing

Our studies confirmed halogenation as a new paradigm for the tailored design and engineering of self-assembling peptides and, in particular, point out the potential impact of iodination when performed on aliphatic residues. Thus, it extends the importance of single atom replacements in the context of peptide-based nanomaterials.

Experimental Section

Peptides synthesis and fibrillation: Peptides employed in the study were synthesized according to the procedure described in the Supporting Information. CTC resin and N-α-Fmoc-L-amino acids used during chain assembly were purchased from Iris Biotech GmbH (Marktredwitz, Germany). Ethylcyanoglyoxylate-2-oxime (Oxyma) was purchased from Novabiochem (Darmstadt, Germany), N,N'-dimethylformamide (DMF) and trifluoroacetic acid (TFA) were from Carlo Erba (Rodano, Italy). N,N'-diisopropylcarbodiimide (DIC), dichloromethane (DCM), and all other organic reagents and solvents, unless stated otherwise, were purchased in high purity from Sigma-Aldrich (Steinheim, Germany). All solvents for solid-phase peptide synthesis (SPPS) were used without further purification. HPLC grade acetonitrile (ACN) and ultrapure 18.2 Ω water (Millipore-Milli-Q) were used for the preparation of buffers solutions for liquid chromatography. The chromatographic columns were from Phenomenex (Torrance CA, U.S.A.). Fibrillation tests were performed by dissolving the peptides as bulk powders in Milli-Q water to obtain solution with 2, 1, 0.75, 0.5, 0.2, and 0.1 mM concentration. Complete dissolution was obtained sonicating for 10 s and gently warming up to 90 °C for D-AllG(I$_2$)-NKF, whereas for D-AllG-NKF mixing by vortex for 30 s was required. DLS analyses were performed to confirm the absence of undissolved aggregates that may have affected the self-assembly. Solutions incubated at room temperature were placed in a water bath at 20 °C up to 72 h, whereas solutions incubated at higher temperature were placed in a water bath at 60 °C for 1 h, then at 20 °C up to 72 h.

Congo Red staining: Peptide solutions used for staining experiments were placed on a glass microscope, allowed to air dry and then stained with a Congo Red solution. An 80 % ethanol solution saturated with NaCl and Congo Red was freshly prepared before each measurement. Samples were analysed using polarised light and monitored for green birefringence using an Olympus BX50 polarising microscope with a SensiCam PCO camera, which was used to display and enhance images.

Attenuated total reflectance-Fourier transformed infrared spectroscopy (ATR-FTIR): ATR-FTIR spectra of dried peptides water solutions were analysed after incubation by using a Nicolet iS50 FTIR spectrometer equipped with an ATR device. For each sample, droplets were dried directly over the ATR crystal to form a film. Spectra were collected in the medium IR region (64 scans, 4000–400 cm^{-1}). All the spectra were measured with a resolution of ± 1 cm^{-1} and corrected for the air background.

Scanning Electron Microscopy (SEM): Scanning electron microscopy (SEM) analysis was performed using a Cambridge Stereoscan 360 operating at 20 kV. Peptide solutions were incubated in water solutions for 72 h, lyophilized, placed on steel stubs and then sputter-coated with gold before analysis.

Transmission Electron Microscopy (TEM): Transmission electron microscopy (TEM) images were collected using JEM 3200FSC field emission microscope (JEOL) operated at 300 kV in bright field mode with Omega-type Zero-loss energy filter. Images were acquired with GATAN DIGITAL MICROGRAPH software. Low resolution TEM images were acquired by using a DeLong America LVEM5, equipped with a field emission gun and operating at 5 kV. 15 µL of each sample were placed on a 200-mesh carbon film-coated grid and the exceeding solvent was removed with filter paper after 1 minute to prevent aggregation effects promoted by drying. The procedure was repeated twice for each grid.

Single crystal X-ray diffraction: Data collections for D-AllG(I$_2$)-NKF were performed at the X-ray diffraction beamline (XRD2) of the Elettra Synchrotron, Trieste (Italy). The crystals were dipped in NHV oil and mounted on the goniometer head with kapton loops. Complete datasets were collected at 100 K (nitrogen stream supplied through an Oxford Cryostream 700) through the rotating crystal method. Data were acquired using a monochromatic wavelength of 0.62 Å, on a Pilatus 6 M hybrid-pixel area detector. The diffraction data were indexed and integrated using XDS. Two different datasets, collected from different crystals randomly oriented, have been merged to obtain a complete set of data. Semi-empirical absorption corrections and scaling were performed on datasets, exploiting multiple measures of symmetry-related reflections, using SADABS program. Crystals of diiodo-allylglycine (AllG(I$_2$)) were measured using Mo-Kα radiation on a Bruker KAPPA APEX II diffractometer. Crystal structure was solved by direct method and refined against F2 using SHELXL97. Packing diagrams were generated using Mercury.

Deposition Numbers 2088436 (for diiodo-allylglycine, AllG(I$_2$)), 2086345 (for D-AllG(I$_2$)-NKF) contain the supplementary crystallographic data for this paper. These data are provided free of charge by the joint Cambridge Crystallographic Data Centre and Fachinformationszentrum Karlsruhe Access Structures service.

Powder X-ray diffraction (PXRD): Powder X-ray diffraction data were collected at r.t. on Bruker AXS D8 powder diffractometer with experimental parameters as follows: Cu–Kα radiation ($\lambda = 1.5418$ Å), scanning interval 3–40° at 2θ, step size 0.015°, exposure time 6 s per step.

Peptide-mediated gold reduction: HAuCl$_4$·3H$_2$O ($>$99.9 %) was purchased from Sigma-Aldrich (Steinheim, Germany). 1 mM peptides' solutions were freshly prepared each time by dissolving peptide powders in Milli-Q water. Complete dissolution was obtained sonicating for 10 s and gently warming up to 90 °C for D-AllG(I$_2$)-NKF, whereas for D-AllG-NKF shaking for 30 s was required. The obtained peptide solution was diluted using 1 mM HAuCl$_4$ solutions to achieve a final concentration of 0.5 mM for both reagents. The peptide/HAuCl$_4$ solutions were subsequently incubated at 60 °C under magnetic stirring for 1 h.

UV spectroscopy: UV-vis spectra of Au-peptide superstructures in Milli-Q water were acquired at room temperature on a Jasco V-630 spectrophotometer equipped with a halogen lamp and a deuterium lamp.

Conflict of Interest

The authors declare no conflict of interest.

Data Availability Statement

The data that support the findings of this study are available in the supplementary material of this article.

[1] A. A. Kermani, *FEBS J.* **2021**, *288*, 5788–5804.
[2] U. B. Gawas, V. K. Mandrekar, M. S. Majik, in *Adv. Biol. Sci. Res.* (Eds: S. N. Meena, M. M. Naik), Elsevier, **2019**, pp. 69–84.
[3] J. L. Parker, S. Newstead, *Protein Sci.* **2013**, *22*, 1664–1668.
[4] Q. Liu, W. A. Hendrickson, *Methods Mol. Biol.* **2017**, *1607*, 377–399.
[5] C. Hou, O. V. Tsodikov, *Acta Crystallogr. Sect. D* **2019**, *75*, 32–40.
[6] A. C. W. Pike, E. F. Garman, T. Krojer, F. Von Delft, E. P. Carpenter, *Acta Crystallogr. Sect. D* **2016**, *72*, 303–318.
[7] W. A. Hendrickson, J. R. Horton, D. M. LeMaster, *EMBO J.* **1990**, *9*, 1665–1672.
[8] Y. Srivastava, R. Bonn-Breach, S. Chavali, G. Lippa, J. Jenkins, J. Wedekind, *Crystals* **2021**, *11*, 273.
[9] T. Li, F. Krumeich, J. Ihli, Z. Ma, T. Ishikawa, A. B. Pinar, J. A. van Bokhoven, *Chem. Commun.* **2019**, *55*, 482–485.
[10] Y. Taguchi, T. Saio, D. Kohda, *J. Phys. Chem. Lett.* **2020**, *11*, 5451–5456.
[11] N. Jakubowski, J. Messerschmidt, M. G. Añorbe, L. Waentig, H. Hayen, P. H. Roos, *J. Anal. At. Spectrom.* **2008**, *23*, 1487–1496.
[12] P. E. Schneggenburger, A. Beerlink, B. Worbs, T. Salditt, U. Diederichsen, *ChemPhysChem* **2009**, *10*, 1567–1576.
[13] U. Rost, Y. Xu, T. Salditt, U. Diederichsen, *ChemPhysChem* **2016**, *17*, 2525–2534.
[14] G. Berger, P. Frangville, F. Meyer, *Chem. Commun.* **2020**, *56*, 4970–4981.
[15] C. Pigliacelli, K. B. Sanjeeva, Nonappa, A. Pizzi, F. B. Bombelli, P. Metrangolo, *ACS Nano* **2019**, *13*, 2158–2166.
[16] C. A. Gunawardana, M. Đaković, C. B. Aakeröy, *Chem. Commun.* **2018**, *54*, 607–610.
[17] Q. Zou, J. Huang, X. Zhang, *Small* **2018**, *14*, 1803101.
[18] J. Gamekkanda, A. Sinha, J. Desper, M. Đaković, C. Aakeröy, *Crystals* **2017**, *7*, 226.
[19] M. Saccone, L. Catalano, *J. Phys. Chem. B* **2019**, *123*, 9281–9290.
[20] B. Li, S. Q. Zang, L. Y. Wang, T. C. W. Mak, *Coord. Chem. Rev.* **2016**, *308*, 1–21.
[21] A. Pizzi, L. Catalano, N. Demitri, V. Dichiarante, G. Terraneo, P. Metrangolo, *Pept. Sci.* **2020**, *112*, e24127.
[22] R. Bertrand, M. Wagner, V. Derdau, O. Plettenburg, *Bioconjugate Chem.* **2016**, *27*, 2281–2286.
[23] G. Cavallo, P. Metrangolo, R. Milani, T. Pilati, A. Priimagi, G. Resnati, G. Terraneo, *Chem. Rev.* **2016**, *116*, 2478–2601.
[24] M. Saccone, V. Dichiarante, A. Forni, A. Goulet-Hanssens, G. Cavallo, J. Vapaavuori, G. Terraneo, C. J. Barrett, G. Resnati, P. Metrangolo, A. Priimagi, *J. Mater. Chem. C* **2015**, *3*, 759–768.
[25] A. Bertolani, L. Pirrie, L. Stefan, N. Houbenov, J. S. Haataja, L. Catalano, G. Terraneo, G. Giancane, L. Valli, R. Milani, O. Ikkala, G. Resnati, P. Metrangolo, *Nat. Commun.* **2015**, *6*, 7574.
[26] S. Kralj, O. Bellotto, E. Parisi, A. M. Garcia, D. Iglesias, S. Semeraro, C. Deganutti, P. D'Andrea, A. V. Vargiu, S. Geremia, R. De Zorzi, S. Marchesan, *ACS Nano* **2020**, *14*, 16951–16961.
[27] A. Bertolani, A. Pizzi, L. Pirrie, L. Gazzera, G. Morra, M. Meli, G. Colombo, A. Genoni, G. Cavallo, G. Terraneo, P. Metrangolo, *Chem. Eur. J.* **2017**, *23*, 2051–2058.
[28] R. K. Spencer, J. S. Nowick, *Isr. J. Chem.* **2015**, *55*, 698–710.
[29] K. Tenidis, M. Waldner, J. Bernhagen, W. Fischle, M. Bergmann, M. Weber, M.-L. Merkle, W. Voelter, H. Brunner, A. Kapurniotu, *J. Mol. Biol.* **2000**, *295*, 1055–1071.
[30] M. Reches, Y. Porat, E. Gazit, *J. Biol. Chem.* **2002**, *277*, 35475–35480.
[31] A. Pizzi, C. Pigliacelli, A. Gori, Nonappa, O. Ikkala, N. Demitri, G. Terraneo, V. Castelletto, I. W. Hamley, F. Baldelli Bombelli, P. Metrangolo, *Nanoscale* **2017**, *9*, 9805–9810.
[32] A. Pizzi, N. Demitri, G. Terraneo, P. Metrangolo, *CrystEngComm* **2018**, *20*, 5321–5326.
[33] A. Pizzi, V. Dichiarante, G. Terraneo, P. Metrangolo, *Pept. Sci.* **2018**, *110*, e23088.
[34] A. Lakshmanan, D. W. Cheong, A. Accardo, E. Di Fabrizio, C. Riekel, C. A. E. Hauser, *Proc. Natl. Acad. Sci. USA* **2013**, *110*, 519–524.
[35] D. B. Ninković, D. P. Malenov, P. V. Petrović, E. N. Brothers, S. Niu, M. B. Hall, M. R. Belić, S. D. Zarić, *Chem. Eur. J.* **2017**, *23*, 11046–11053.
[36] K. A. Houton, K. L. Morris, L. Chen, M. Schmidtmann, J. T. A. Jones, L. C. Serpell, G. O. Lloyd, D. J. Adams, *Langmuir* **2012**, *28*, 9797–9806.
[37] E. R. Draper, K. L. Morris, M. A. Little, J. Raeburn, C. Colquhoun, E. R. Cross, T. O. McDonald, L. C. Serpell, D. J. Adams, *CrystEngComm* **2015**, *17*, 8047–8057.
[38] J. Wang, K. Liu, R. Xing, X. Yan, *Chem. Soc. Rev.* **2016**, *45*, 5589–5604.
[39] T. Arvinte, A. Cudd, A. F. Drake, *J. Biol. Chem.* **1993**, *268*, 6415–6422.
[40] I. M. Stanković, S. Niu, M. B. Hall, S. D. Zarić, *Int. J. Biol. Macromol.* **2020**, *156*, 949–959.
[41] E. Gazit, *FEBS J.* **2005**, *272*, 5971–5978.
[42] E. Mayans, C. Alemán, *Molecules* **2020**, *25*, 6037.
[43] B. Dalhus, C. H. Görbitz, *Acta Crystallogr. Sect. B* **2000**, *56*, 715–719.
[44] E. Gazit, *Prion* **2007**, *1*, 32–35.
[45] A. J. Howie, D. B. Brewer, D. Howell, A. P. Jones, *Lab. Invest.* **2008**, *88*, 232–242.
[46] A. Shtainfeld, T. Sheynis, R. Jelinek, *Biochemistry* **2010**, *49*, 5299–5307.
[47] M. Groenning, *J. Chem. Biol.* **2010**, *3*, 1–18.
[48] S. Bhattacharjee, G. Tóth, S. Lovas, J. D. Hirst, *J. Phys. Chem. B* **2003**, *107*, 8682–8688.
[49] A. V. Cunha, E. Salamatova, R. Bloem, S. J. Roeters, S. Woutersen, M. S. Pshenichnikov, T. L. C. Jansen, *J. Phys. Chem. Lett.* **2017**, *8*, 2438–2444.
[50] D. A. Middleton, J. Madine, V. Castelletto, I. W. Hamley, *Angew. Chem. Int. Ed.* **2013**, *52*, 10537–10540; *Angew. Chem.* **2013**, *125*, 10731–10734.
[51] E. Chatani, N. Yamamoto, *Biophys. Rev. Lett.* **2018**, *10*, 527–534.
[52] A. K. Buell, *Biochem. J.* **2019**, *476*, 2677–2703.
[53] R. Riek, *Cold Spring Harbor Perspect. Biol.* **2017**, *9*, a023572.
[54] M. R. Sawaya, S. Sambashivan, R. Nelson, M. I. Ivanova, S. A. Sievers, M. I. Apostol, M. J. Thompson, M. Balbirnie, J. J. W. Wiltzius, H. T. McFarlane, A. Madsen, C. Riekel, D. Eisenberg, *Nature* **2007**, *447*, 453–457.
[55] J. C. Stroud, *Acta Crystallogr. Sect. D* **2013**, *69*, 540–545.
[56] D. Cannon, A. M. Donald, *Soft Matter* **2013**, *9*, 2852–2857.
[57] M. Lepère, C. Chevallard, G. Brezesinski, M. Goldmann, P. Guenoun, *Angew. Chem.* **2009**, *121*, 5105–5109; *Angew. Chem. Int. Ed.* **2009**, *48*, 5005–5009.
[58] K.-I. Min, D.-H. Kim, H.-J. Lee, L. Lin, D.-P. Kim, *Angew. Chem.* **2018**, *130*, 5732–5736; *Angew. Chem. Int. Ed.* **2018**, *57*, 5630–5634.
[59] Y. Li, Z. Tang, P. N. Prasad, M. R. Knecht, M. T. Swihart, *Nanoscale* **2014**, *6*, 3165–3172.
[60] R. Jain, G. Khandelwal, S. Roy, *Langmuir* **2019**, *35*, 5878–5889.
[61] M. F. Matus, S. Malola, H. Häkkinen, *ACS Nanosci. Au* **2021**, *1*, 47–60.
[62] J. Lu, Y. Xue, K. Bernardino, N.-N. Zhang, W. R. Gomes, N. S. Ramesar, S. Liu, Z. Hu, T. Sun, A. F. de Moura, N. A. Kotov, K. Liu, *Science* **2021**, *371*, 1368–1374.
[63] L. Bellucci, A. Ardèvol, M. Parrinello, H. Lutz, H. Lu, T. Weidner, S. Corni, *Nanoscale* **2016**, *8*, 8737–8748.
[64] T. John, A. Gladytz, C. Kubeil, L. L. Martin, H. J. Risselada, B. Abel, *Nanoscale* **2018**, *10*, 20894–20913.
[65] A. K. Das, C. R. Raj, *J. Phys. Chem. C* **2011**, *115*, 21041–21046.
[66] P. S. D. Robinson, G. N. Khairallah, G. da Silva, H. Lioe, R. A. J. O'Hair, *Angew. Chem. Int. Ed.* **2012**, *51*, 3812–3817; *Angew. Chem.* **2012**, *124*, 3878–3883.
[67] A. Nijamudheen, A. Datta, *Chem. Eur. J.* **2020**, *26*, 1442–1487.
[68] R. A. Daley, A. S. Morrenzin, S. R. Neufeldt, J. J. Topczewski, *J. Am. Chem. Soc.* **2020**, *142*, 13210–13218.